Electrochimica Acta 210 (2016) 606–614

Contents lists available at ScienceDirect

Electrochimica Acta

journal homepage: www.elsevier.com/locate/electacta

Mesoporous films prepared from synthesized TiO_2 nanoparticles and their application in dye-sensitized solar cells (DSSCs)

Nikola Tasić[a,*], Zorica Marinković Stanojević[a], Zorica Branković[a], Uroš Lačnjevac[a], Vesna Ribić[a], Milan Žunić[b], Tatjana Novaković[c], Matejka Podlogar[d], Goran Branković[a]

[a] Institute for Multidisciplinary Research, Department of Materials Science, University of Belgrade, Kneza Višeslava 1, 11000 Belgrade, Serbia
[b] Department of Basic Sciences, College of Engineering and Information Technology, University of Business and Technology, P.O. Box 11020, Jeddah 21361, Saudi Arabia
[c] IChTM-Department of Catalysis and Chemical Engineering, University of Belgrade, Njegoševa 12, 11000 Belgrade, Serbia
[d] Jožef Stefan Institute, Jamova cesta 39, SI-1000 Ljubljana, Slovenia

ARTICLE INFO

Article history:
Received 13 January 2016
Received in revised form 26 May 2016
Accepted 26 May 2016
Available online 27 May 2016

Keywords:
Dye-sensitized solar cells (DSSCs)
TiO_2 photoanode
EDTA-Na_2
Triton X100
Electrochemical Impedance Spectroscopy (EIS)

ABSTRACT

In this paper, we propose a novel method for preparation of high surface area titania nanoparticles, and investigate their photovoltaic performance in dye sensitized solar cells (DSSCs). The precursor compound titanium(IV)-isopropoxide is hydrolyzed in the presence of nonionic surfactant (Triton X100) and ethylenediaminetetraacetic acid sodium salt (EDTA-Na_2) and thermally transformed into gel. The gel is autoclaved, resulting in submicronic micelles which are further processed into mesoporous films. The films are deposited from paste, composed of ultrasonically broken micelles and the organic ingredients. The crack-free film structures, composed of sub–25 nm pure anatase particles are observed using the appropriate instrumental techniques: scanning electron microscopy (SEM), field-emission scanning electron microscopy (FE-SEM), transmission electron microscopy (TEM), X-ray diffractometry (XRD), UV-VIS-NIR spectroscopy. The large surface area of 158 $m^2 g^{-1}$ and mesoporosity are confirmed using the data obtained from the nitrogen adsorption-desorption isotherm. The photovoltaic performance of the operating N719-sensitized solar devices are tested using electrochemical impedance spectroscopy (EIS), open-circuit voltage decay (OCVD) and by recording current density-voltage (J-V) curves. The cell exhibits promising photocurrent density up to 11.7 mA cm^{-2}, and the photo-to-electric power efficiency of 5.22%, for cell area of 0.24 cm^2, under 100 mW cm^{-2} halogen light source.

1. Introduction

Dye-sensitized solar cells (DSSCs) are recognized as a cost-effective alternative to the conventional silicon photovoltaic devices [1,2], owing to wide availability and non-toxicity of its key component, titanium(IV)-oxide. For the past two decades, these 3rd generation photovoltaic devices have been under extensive investigation, with the highest reported light-to-current conversion efficiencies of 14.3% for the cell area of 0.1024 cm^2 [3] and 11.9% for the cell area of 1.005 cm^2 [4], which are comparable to the efficiencies of other thin film photovoltaics, such as amorphous-Si ($10.1 \pm 0.3\%$, 1.036 cm^2), copper zinc tin sulphur selenide (CZTSS) ($12.6 \pm 0.3\%$, 0.4209 cm^2) or the emerging organic solar cells ($10.7 \pm 0.3\%$, 1.013 cm^2) [3]. In order to approach the theoretical efficiency limit [5,6], increase the reproducibility and expand the large scale production of DSSCs [7], current research is either focused on the synthesis of more efficient light-harvesting dyes [8,9], the optimization of the photoactive electrode, or the innovative cell configurations [10–14].

The typical photoactive electrode is composed of mesoporous TiO_2 film with the high internal surface, onto which a monolayer of the photosensitive dye is adsorbed. Hydrothermal preparation of TiO_2 colloidal dispersions, and their processing into such films using screen-printing or doctor blade deposition, has emerged as the most suitable concept. It provides a much more reproducible and controlled porous high surface area nanotexture, while satisfying future production requirements [15].

The precursor solution in these procedures typically consists of Ti – compound or/and commercially available TiO_2 powder which is/are further autoclaved at the temperatures up to 270 °C, resulting in highly-ordered or randomly oriented mesoporous networks, consisting of microspheres [16], nanospheres [17], or

* Corresponding author. Tel.: +381 112085059; fax: +381 112085038.
E-mail address: nikola.tasic@imsi.bg.ac.rs (N. Tasić).

http://dx.doi.org/10.1016/j.electacta.2016.05.179
0013-4686/

nanotubes [18,19], or the uniform monolith structures, which have exhibited superior photovoltaic results [20,21].

In recent years, there were several reports on modified practice, involving the presence of sophisticated organic compounds in the precursor solution, such as surfactants, templates or strong bases, which promote stabilization during the process of formation and hydrothermal growth of nanoparticles, and also contribute to the morphological properties of the particles [22–26].

Ethylenediaminetetraacetic acid sodium salt (EDTA-Na_2) is a hexadentate ligand. In recent years, its chelating and capping abilities have been recognized in the field of nanostructured materials, with the role as a chelating agent or structure directing agent [27–33], but with no reports of its usage in DSSCs related research.

Polyoxyethylene octyl phenyl ether, commercially available as Triton X100, has been commonly utilized in preparation of nanopowder pastes, to promote the spreading of paste upon the deposition [34], or for dispersion purposes [35,36]. For the best of our knowledge, there is only one report of the usage of this surfactant in the TiO_2 pre-autoclaving solution, resulting in well dispersed particles with an average size of 20 nm, and subsequently, 4.9–5.2% efficiency for a 10 μm thick film, sensitized with N719 dye [24].

In this paper, as a continuation of our DSSCs related research [37], we propose a hydrothermally assisted sol-gel synthetic route, which builds on the combined impact of the nonionic surfactant, Triton X100, and the chelating agent, EDTA-Na_2 that leads to the formation of high-surface area nanoanatase particles with rice-like shape. The role of the chelating agent was to prevent typically rapid precipitation of the monomeric titanium(IV)-isopropoxide precursor during the sol-gel stage of the synthesis, through the formation of water soluble complex, and to direct the shape of the primary particles during the hydrothermal growth. On the other side, the surfactant was introduced into the reaction mixture in order to prevent the excessive particles growth during the autoclaving, through the formation of easily processible submicronic micelles. Furthermore, as synthesized micelles were ultrasonically broken into primary particles and processed into mesoporous films which were used for fabrication of N-719-sensitized solar cells. We present thorough electrical characterization of fabricated DSSCs, with the special attention on the electronic processes in the operating photovoltaic devices, and the reproducibility of the method.

2. Experimental

2.1. Synthesis of titania nanoparticles and film preparation

Titanium(IV)-isopropoxide (TTIP, Alfa Aesar, 97% min), Triton X100 (TX100, J.T. Baker) and iso-propanol (i-PA, AnalaR NORMAPUR, VWR) were mixed in the molar ratio of 1:1:40, and mildly stirred to dissolve the complete amount of TX100. Then, 80 mM aqueous solution of EDTA-Na_2 (Aldrich Chemistry, molar ratio TTIP:EDTA-Na_2 = 4:1) was slowly added into the stirring mixture. After the whole portion of EDTA-Na_2 was added, the temperature was raised and held at 80 °C for 3 h, during which the peptization process was carried out. The formed yellowish viscous precipitate was mixed with 20 ml of distilled H_2O, and transferred into the stainless steel autoclave for hydrothermal treatment (Carl Roth, Model II, high-pressure autoclave). The temperature was adjusted and held at 200 °C for 18 h, during which the pressure arised to approximately 10 bar. After the hydrothermal treatment, the formed gel was centrifuged and rinsed several times using absolute ethanol with sonication. Paste was prepared by the addition of the organic agents and homogenized using the ultrasound horn (Bandelin Sonoplus 2070HD). We have used α-terpineol (95% min, Alfa Aesar) as a dispersant, ethyl-cellulose (viscosity 4 cP, Aldrich Chemistry) as a binder, and the combination of acetic acid (MOS HEMOS, pro analysi) and distilled water as adhesion agents, strongly following the previously proposed procedure and the ingredients shares [38]. The exact compostion of the paste was as follows: rinced product of hydrothermal synthesis (1.6 g, of which 0.24 g corresponded to TiO_2), glacial acetic acid (0.24 g), H_2O (0.60 g), α-terpineol (1.40 ml), ethyl-cellulose (0.20 g).

The deposition on the cleaned FTO substrates (MTI Crystal, 12–14 Ω/sq) was carried out using a doctor blade film applicator with the green sheet thickness of 40 μm. The drying and the calcination processes on the titanium hot plate were carefully designed to prevent the formation of cracks. This was achieved by the slow increase of temperature from ambient conditions to 500 °C, at which the films were held for 10 min. Then, the films were immersed in a 50 mM aqueous solution of $TiCl_4$ (Aldrich Chemistry), and thermally treated at 80 °C for 40 minutes, followed by another drying and calcination treatment (500 °C/10 min). The chemical bath deposition of $TiCl_4$ was performed in order to improve binding of dye onto the TiO_2 surface, and/or to induce important effects on recombination, surface electric field and charge transport, which increase photocurrent density of the operating cell [39,40].

2.2. DSSC assembly

The re-calcined films were cooled to 70 °C and immersed in 0.5 mM solution of cis-bis(isothiocyanato)bis(2,2′-bipyridyl-4,4′-dicarboxylato)-ruthenium(II)bis-tetrabutylammonium (Solaronix, N719) ethanol solution for 24 h. The counter-electrode was prepared by doctor-blade deposition of Pt paste (Platisol T/SP, Solaronix) onto FTO glass (MTI Crystal, 12–14 Ω/sq) and calcinated at 450 °C/15 min in the chamber furnace. The dye-covered electrodes and Pt counter electrodes were assembled into a sandwich-type cell and sealed with the binder clips. Finally, the assembled cell was filled with the electrolyte containing the I^-/I^{3-} redox system (Iodolyte 50, Solaronix) by dripping several drops between the electrodes.

2.3. Characterization of TiO_2 photoanodes and DSSCs

Thorough morphological analysis of the deposited films was performed using scanning electron microscopy (SEM, VEGA3 TESCAN), field-emission scanning electron microscopy (FESEM, MIRA3 TESCAN) and transmission electron microscopy (TEM, JEM-2100 JEOL). The crystallographic structure of synthetized material was investigated on Rigaku RINT 2000 diffractometer with parafocal Bragg–Brentano geometry, using Cu Ka radiation (k = 1.54178 Å). Also, the selected-area electron diffraction (SAED) pattern of the scratched film is presented. The nitrogen adsorption on the scratched films sample was performed at −196 °C and relative pressure interval between 0.05 and 0.98 in automatic adsorption apparatus (Sorptomatic 1990 Thermo Finningen). Before each measurement, the sample was degassed at 200 °C under vacuum for long enough time to observe the absence of significant changes in vacuum stability ($4\,h < t < 10\,h$). The adsorbed amount of nitrogen was measured by volume at standard temperature and pressure. The specific surface area S_{BET} was calculated by the BET method [41–43] from nitrogen adsorption–desorption isotherms, using data up to $p/p_o = 0.3$, and the pore size distribution have been computed from desorption branch of the isotherms [43]. The optical properties of the synthesized material were analyzed using a UV-2600 Shimadzu spectrophotometer with the integrated sphere. For the photovoltaic measurements, the fabricated cells were illuminated with an Osram 120 V/300 W

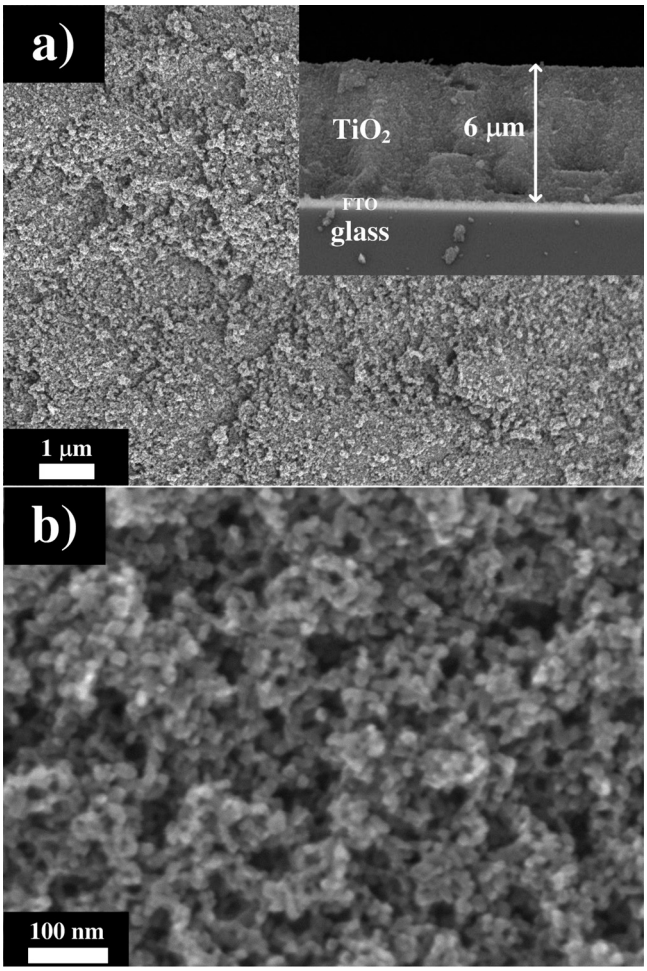

Fig. 1. (a) Morphology of as prepared $TiCl_4$ treated-TiO_2 film. (b) High magnification FE-SEM image of the mesoporous TiO_2 structure. Inset in (a) shows the SEM image of the cross-section of the film.

ELH halogen light source at 100 mWm^{-2}, simulating AM1.5 spectrum, and their current density–voltage characteristics were registered with a Keithley 237 Sourcemeter (V–I sweep mode, range 0–0.80 V, step 0.01 V, delay time 0.040s). For calibration purposes we have used a Volcraft PL-110SM photometer. In order to determine the precise active area, cells were scanned in 1:1 scale using an image scanner, and area was calculated using software area tool. Electrochemical impedance spectroscopy (EIS) measurements were carried out at two cell voltages, 0.7 V (open-circuit voltage, V_{OC}) and 0.8 V, in the dark and under illumination, by means of a Reference 600 potentiostat and EIS 300 software (Gamry Instruments, USA). Impedance spectra were recorded by applying the amplitude of 10 mV RMS over a wide frequency range from 10^6 to 0.1 Hz with 20 points per decade. The complex nonlinear least squares (CNLS) method was applied for fitting the equivalent circuit parameters to the spectra using the Gamry Echem Analyst software, version 6.25. The open-circuit voltage decay measurements (OCVD) were performed on the Keithley 237 Sourcemeter, by recording I–V sweep curves on the constant current level (0.000 nA, open-circuit conditions, 5 seconds delay between the measured points), upon the termination of light (0 mW cm^{-2}).

3. Results and Discussion

A uniform, crack-free structure, and rough surface of as-synthesized films can be observed in a low magnification FE-SEM micrograph (Fig. 1a), while the high resolution FE-SEM analysis (Fig. 1b) reveals a highly porous structure, consisting of randomly oriented particles. The overall mesoporosity (i.e. pores diameter 2–50 nm) is one of the crucial demands for obtaining full dye and electrolyte distribution within the film, and subsequently, promising photovoltaic response. In our case, the obvious porosity can be attributed to ethyl-cellulose:TiO_2 mass ratio in the paste (1:1.2), combined with the effective ultrasonic paste homogenization after the binder addition (30 min at 70 W) and a moderate thermal decomposition of the organics.

Additionally, as-synthesized films exhibit high transparency and pale yellow tint when exposed to light. The chemical bath deposition of $TiCl_4$, performed after the first deposition/calcination treatment, has led to the impregnation and the outstanding adhesion of the films. The thickness of the film deposited in one deposition/calcination cycle is approx. 6 μm, according to the SEM cross-section micrograph, presented in the inset of Fig. 1a. Furthermore, the microscopic analysis of the the cross-section confirms that the nanosized particles are connected into the extended semiconducting network, vital for the fluent charge transport during the solar cell operation.

More informations on the dimensions and porosity of the synthesized material derive from the N_2 adsorption-desorption isotherm and pore size distribution curve of the scratched film sample (Fig. 2). The sample exhibits isotherm type IVa, with hysteresis loop of the H1 type (Fig. 2a). Type IVa isotherm is encountered when adsorption occurs on low porosity materials or on materials with mostly mesoporous pore diameters, such as in

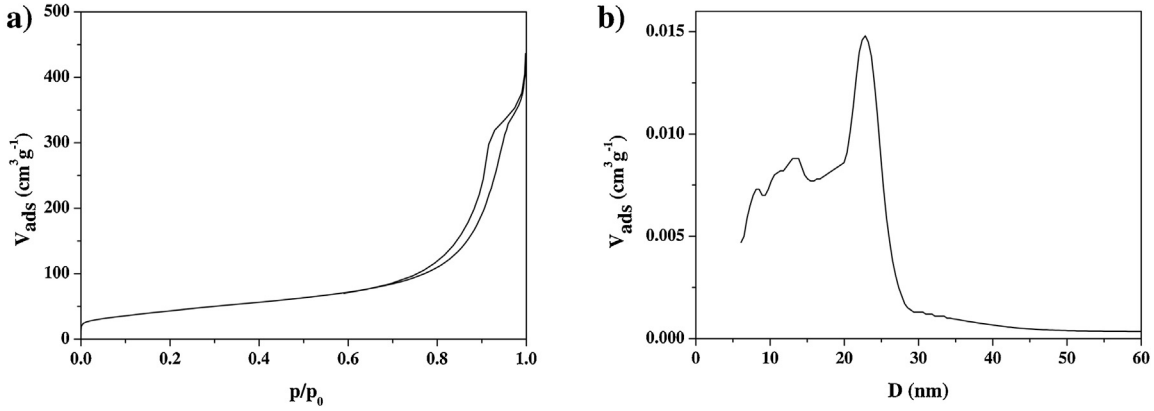

Fig. 2. (a) N_2 adsorption-desorption isotherm. (b) Pore-size distribution curve. The analysis was performed on the scratched film sample.

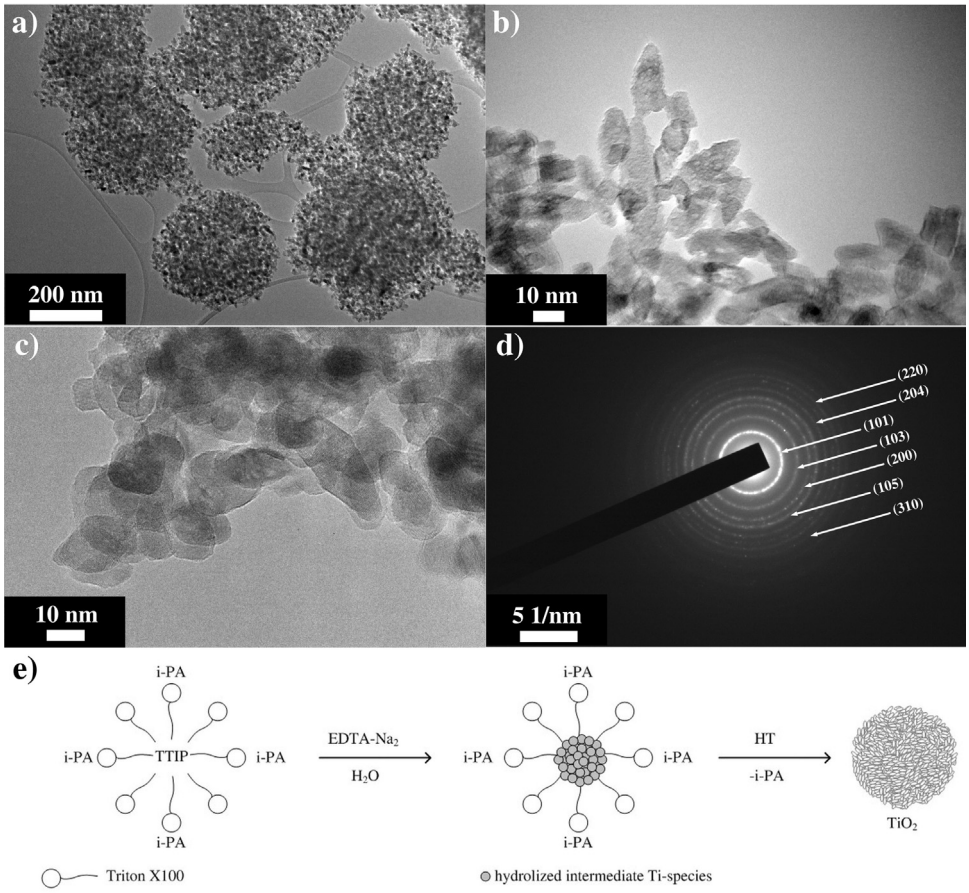

Fig. 3. (a) TEM image of the raw product after the hydrothermal treatment; the dense micellar stabilization of the primary particles has occured due to the presence of nonionic surfactant, Triton X100. (b) Primary particles at the edges of micelles. (c) TEM image of scratched film sample; small dimensions were preserved during the calcination of the films. (d) SAED pattern of the scratched films sample, typical for polycrystalline anatase samples. (e) Proposed particles formation mechanism during the synthesis.

our case. The mesoporosity is characterized by the capillary condensation step in the isotherm between relative pressures of 0.5 and 0.8. The sharp steps in the isotherms suggest that capillary condensation occurs in a narrow range of mesopores [41–43].

The pore size distribution curve exhibits a sharp, dominant peak at approximately 22.8 nm, two combined peaks at 13.4 nm and 10.9 nm, and one low pore volume peak at 8.1 nm. Considering that the average dye molecule size is approximately 1.5 nm [20], fluent electrolyte transport and facile penetration throughout the electrode interior can be expected, despite the non-uniformity of the pore size distribution.

In addition, the calculated specific surface area of TiO_2 nanoparticles is 158 m^2/g, which is an outstanding feature of the synthesized material, considering that it is significantly higher than those of the commercially available and widely utilized titania powders (Degussa P25 – 56 m^2/g, Sigma-Aldrich nano-anatase – 55 m^2/g). The large surface area is a desirable property from the perspective of photovoltaic application, because it enables high uptake of dye, and consequently, enhanced photo-current response.

Furthermore, the raw product of the hydrothermal synthesis and the scratched film sample were analyzed using TEM (Figs. 3a-d), to determine the shape and dimensions of the nanosized particles at different stages of the synthesis. Also, the analyses were used to propose the mechanism of the particles formation, presented in Fig. 3e. The particles at the edges of the hydrothermally formed micelles exhibit rice-like shape barely exceeding 25 nm in length, and 15 nm in width (Fig. 3b). On the other side, the analysis of the scratched film sample (Fig. 3c) showed that the dimensions of the particles were not affected by the calcination treatment. We assume that the rice-like shape (Fig. 3b and 3c), along with the large surface area of the nanosized particles could be a consequence of the cooperation effect between EDTA-Na_2 and Triton X100, during the synthesis. A similar effect between EDTA and oleic acid, as surfactant, has been reported previously, resulting in nanoarchitectures consisting of EDTA-structure-directed-particles [32]. In the case of this study, the presence of EDTA-Na_2 has obstructed the hydrolysis of the titanium(IV)-isopropoxide, and the immediate precipitation of hydrolyzed titanium species. Most likely, the intermediate structures between a strong ligand (EDTA) and titanium species were formed, where the presence of ligand affected the growth of particles, leading to their elongated shape. Assumably, during the evaporation of iso-propanol, some of the alcohol species that surround the metalic cations were eventually replaced with the strong ligand (EDTA), and two additional bonds with the ligand were formed. The formation of the bonds between ligand and titanium has lead to the change of the titanium coordination number from 4 to 6, resulting in the octahedral environment of Ti^{4+}-ion [44]. This change of the coordination number directs the final shape of the forming elongated nanoparticles. After the formation of the octahedral intermediate complex, the complex links with the oxyethylene and/or −OH group of the non-ionic Triton X100 micelles, previously formed with the addition of water [45].

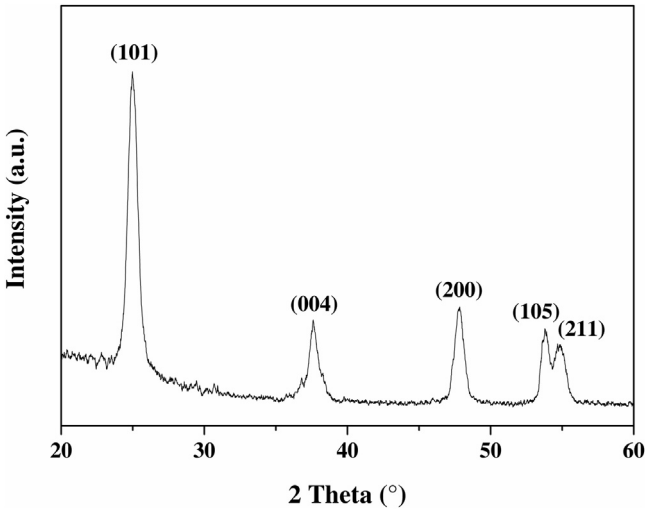

Fig. 4. XRD pattern of the calcined titania paste.

Finally, finite capacity of the micelles limitates further growth of the particles, which after autoclaving barely exceed 20 nm in length.

Furthermore, TEM analysis was used to determine the crystallographic nature of the scratched film sample by means of SAED technique (Fig. 3d). Seven distinctive circles were observed, corresponding to (101), (103), (200), (105), (204), (220), and (310) anatase crystallograhic planes. Another confirmation of the anatase presence comes from the XRD analysis, performed on the calcined paste sample (Fig. 4).

The wide diffraction peaks presented in Fig. 4 correspond to (101), (004), (200), (105) and (211) anatase crystallographic planes, in agreement to JCPDS 21-1272. From the perspective of application in DSSCs, anatase is a preferred crystallographic structure, according to the comparative study between anatase- and rutile- based cells, with up to 30% higher photocurrents [46]. The superior anatase behavior is attributed to the more favorable structure and chemical composition of its surface, than in the other TiO_2 polymorphs. The formation of the anatase phase could be a result of the acidic conditions during the synthesis (pH 5.5) and the low temperature and short duration of calcination step (500 °C/10 min). We emphasize that no pH adjustment was performed during the synthesis, and that the reaction mixture consisted only of above listed reagents.

The optical properties of the TiO_2 films were investigated by recording UV–vis diffuse reflectance and transmittance spectra

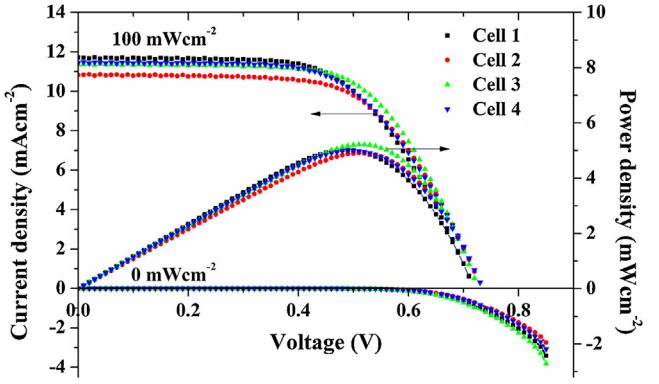

Fig. 6. Photocurrent-density – voltage characteristics of the devices in dark and under 100 mW cm^{-2} simulated AM1.5 illumination, and the corresponding power density – voltage curves for the illuminated devices.

(Fig. 5). The band-gap energy was calculated using Kubelka-Munk transformation and Tauc linearization [47,48] on the diffuse reflectance data (Fig. 5a). The calculated value of the band-gap for TiO_2 sample is 3.17 eV, which is in good accordance with the theoretical value of 3.2 eV for anatase TiO_2.

Additionally, transparency of the films (Fig. 5b) is strongly influenced by the duration and applied power during the ultrasound rinsing of the raw product, after the autoclaving, and ultrasound homogenization of the TiO_2 paste, prior to film deposition. Following the conclusions of other studies, in which the best photovoltaic performance was obtained [38] or can be expected with highly transparent films, due to the higher light harvesting efficiency [49], we have tuned the transmittance to ~50–70% in the visible portion of the spectrum, and used such films for device fabrication.

The photovoltaic performance of fabricated devices was investigated by recording the current density–voltage curves, under the halogen light source at 100 mW cm^{-2}, simulating the AM1.5 spectrum (Fig. 6). Four identical cells, made of 6 μm titania/N719 electrodes, were investigated in order to obtain the operating photovotaic parameters (open-circuit voltage, V_{OC}, short-circuit current density, J_{SC}, fill factor, *FF*, and photo-to-current efficiency, η), and to confirm the reproducibility of the presented synthetic and processing method. The cells exhibit short-current density in the range of 10.825–11.708 mA cm^{-2}, for the circular cell area of 0.24 cm^2. The open-circuit voltage of the cells is in the range of 0.71–0.73 V, typical for anatase-based cells, while the overall efficiencies are in the range of 4.92–5.22%.

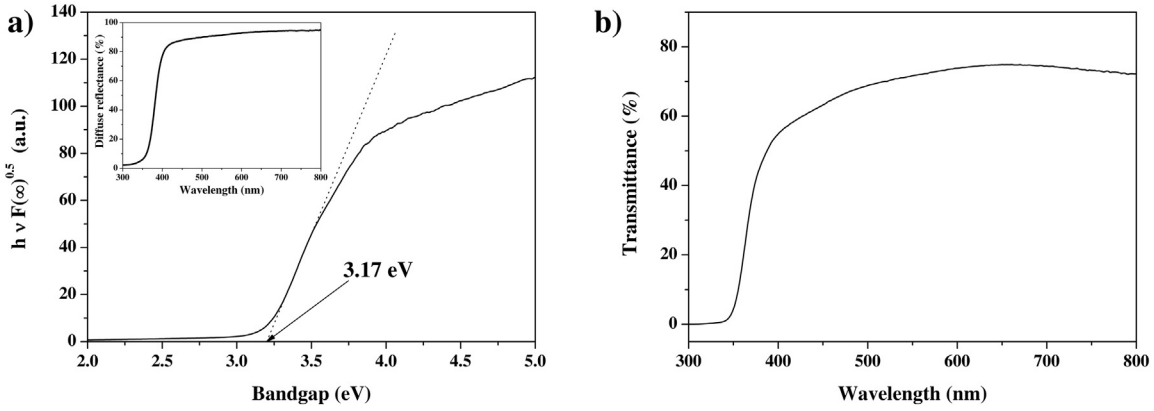

Fig. 5. Optical properties of TiO_2 samples: (a) Optical band-gap of the calcined paste calculated by Kubelka-Munk and Tauc linearization for indirect allowed transition (diffuse reflectance spectrum is presented in inset). (b) Transmittance spectrum of TiO_2 film.

Table 1
The operating parameters of the DSSCs with 6 μm titania/N719 photoanode.

Cell	V_{OC}/V	I_{SC}/mA	J_{SC}/mAcm^{-2}	*FF*	η/%
1	0.71	2.810	11.708	0.603	5.01
2	0.73	2.598	10.825	0.622	4.92
3	0.72	2.728	11.367	0.638	5.22
4	0.73	2.746	11.442	0.599	5.00
Average	0.72	2.720	11.336	0.616	5.04
Standard deviation	0.00957	0.0889	0.370	0.0180	0.128

According to the standard deviation statistics, presented in Table 1, variations of the operating parameters are negligible enough to lead to the conclusion that our results are reproductive. Small differences in the operating parameters are consequence of the fabrication procedure, which includes synthesis of the titania, processing of titania into films, calcination, titanium(IV)-chloride treatment, post-calcination, dye adsorption and preparation of other cell components.

In order to investigate the charge transport phenomena in the operating device and to calculate the electron lifetime, electrochemical impedance spectroscopy (EIS) measurements were performed at two different voltages, 0.7 V (OCV) and 0.8 V, in the dark and under illumination. The impedance responses, corresponding to Cell 1, are given in Fig. 7 as Nyquist plots (a) and Bode plots (b). Experimental data are represented with symbols, while theoretical curves obtained from the CNLS fitting procedure are represented with solid lines. Both of the Nyquist plots recorded at 0.7 V are characterized by four partially overlapping semicircles corresponding to the impedance response of different interfaces and charge transport phenomena in the investigated DSSC device. The best fits were achieved using the equivalent circuit shown in Fig. 7c, which represents a simplified version of general transmission line models used to describe the overall charge transport processes that may occur in DSSCs [50]. In this circuit R_s is the ohmic resistance, whereas the impedance behavior of each interface is represented by a resistance R in parallel with a constant phase element (CPE). The small semicircle observed at high frequencies (10^4–10^5 Hz), shown in the inset of Fig. 7a, is most probably related to the resistance and dielectric properties of the TiO_2 film (R_f||CPE$_f$), while two, much larger semicircles appearing in the intermediate frequency region (10^2–10^4 Hz and 10^1–10^2 Hz) frequency region can be assigned to the charge transfer processes at the counter electrode/electrolyte interface (R_{ce}||CPE$_{ce}$) and the electrolyte/dye/TiO_2 interface (R_{ct}||CPE$_{int}$), respectively. The Nyquist plots also feature

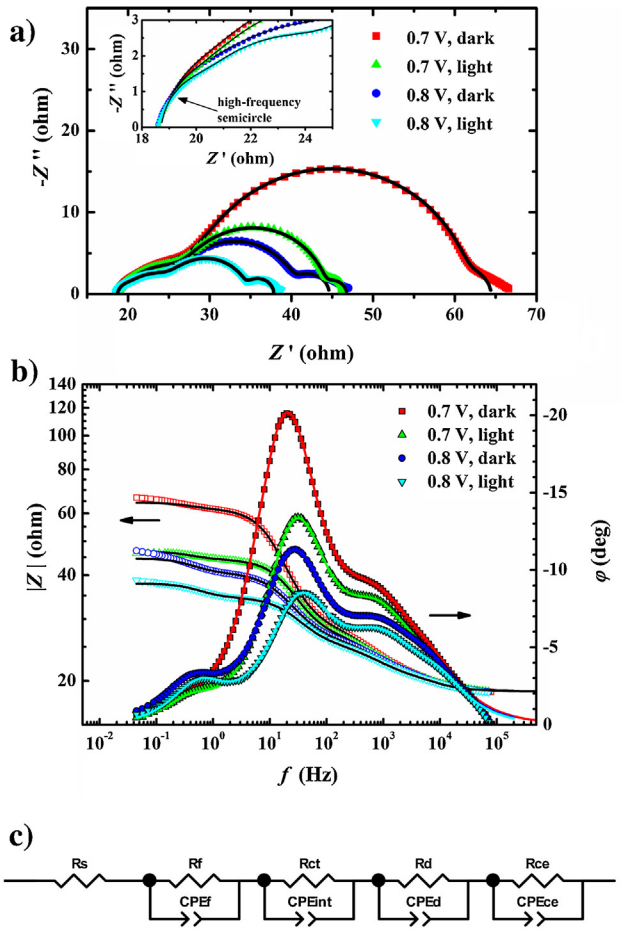

Fig. 7. Impedance spectra of the investigated DSSC recorded at two different voltages, 0.7 V (OCV) and 0.8 V, in the dark and under 100 mW cm^{-2} illumination (marked in the figure), presented using: (a) Nyquist plots and (b) Bode plots. Inset in (a) shows a small semicircle observed at high frequencies. (c) Equivalent circuit used in the CNLS fitting procedure.

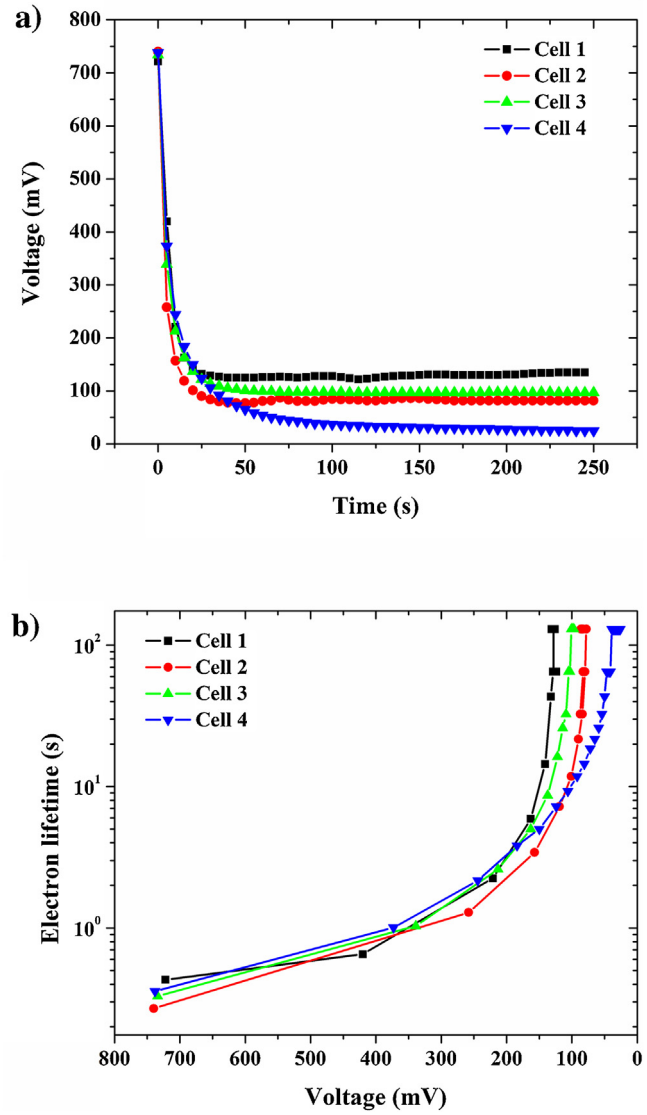

Fig. 8. (a) Open-circuit voltage vs. time curve. (b) Electron lifetime vs. voltage curves obtained by manipulating data from Fig. 8a.

an additional, small semicircle at the lowest applied frequencies (10^{-1}–10^{1} Hz) corresponding to the diffusion of I_3^- ions in the electrolyte, which was modeled by the $R_d||CPE_d$ element. It can be seen from Fig. 8a that the resistance R_{ct} corresponding to the reduction of triiodide ions by electrons transferred from the conduction band of TiO_2 is considerably decreased upon illuminating the device at a constant voltage. At the same time, the apex of this semicircle is shifted towards higher frequencies (Fig. 7b). This can be primarily associated with an increase in the local concentration of I_3^- ions in the pores, caused by the regeneration of the photo-excited dye through the oxidation of I^- to I_3^-, which promotes the recapture of TiO_2 conduction band electrons and diminishes their lifetime [50]. On the other hand, I_3^- reduction is also accelerated to a certain extent due to heating of the cell by the halogen lamp [51]. At voltages higher than the OCV the electron recombination kinetics is significantly improved, accounting for the reduction of the $R_{ct}||CPE_{int}$ semicircle and enlargement of the diffusion semicircle in the Nyquist plots recorded at 0.8 V. Values of the circuit resistances obtained from the CNLS fitting for different experimental conditions are listed in Table 2. The frequencies corresponding to the maxima of $R_{ct}||CPE_{int}$ semicircles, f_{max}, were used to calculate the electron lifetime according to the well-known equation:

$$\tau_{el} = \frac{1}{2\pi \cdot f_{max}} \quad (1)$$

previously reported in literature [52,53].

As can be seen, at both examined voltages the value of τ_{el} for the illuminated device is nearly halved compared with that for the dark cell (Table 2). In general, the values of electron lifetime are system dependent and in our case influenced by the fact that neither the spacer, nor the passivating [54] and scattering layers [55] were used for the device fabrication. Nevertheless, the obtained values are comparable to literature data for the spacer-sealed cells with similar uniform nanocrystalline structure [52], or 154 m^2g^{-1} surface area 3D nanoarchitecture [53].

Furthermore, we have performed the open-circuit voltage decay measurements (OCVD), a popular method which provides informations about the recombination process between the injected electrons in TiO_2 and the electrolyte under the dark state [56–59].

Open-circuit voltage versus time curves are presented in Fig. 8a, showing the exponential decay of voltage, after the interruption of light (sudden switch from 100 to 0 mW cm^{-2}), because of the internal trapping/detrapping [57,59]. Due to the absence of the spacer between the photoelectrode and platinum counter electrode, only ~20 seconds were enough to achieve decay of the open-circuit voltage value to the constant low voltage level, which ranges from 25 (Cell 4) to 135 mV (Cell 1). Test period of 250 seconds (5 seconds between the measuring points) was enough to demonstrate high resolution electron lifetime vs. voltage curves, where the lifetime was calculated according to the following equation [58,60,61]:

$$\tau_{OCVD} = \frac{-k_B T}{e} \cdot \left[\frac{dV_{OC}}{dt}\right]^{-1} \quad (2)$$

Curves exhibit two distinctive parts. The first one is exponential increase of the lifetime at high V_{OC}, upon the interruption of light and initial voltage decay, attributed to the trapping/detrapping of the electrons [57]. The second one is the linear increase of lifetimes in low V_{OC} region, which is governed by the bulk traps that capture the injected electrons [57,59]. The cells (1-4) exhibit high electron lifetimes at open-circuit voltage conditions prior to light termination: 0.430 s, 0.270 s, 0.329 s and 0.356 s, respectively. The values are larger than those from EIS measurements, due to the difference in definition of lifetime. The electron lifetime obtained from EIS is an interpretation of the fitted semicircle attributed to semiconductor/dye/electrolyte interface, while the value from OCVD measurements is an unambigous parameter, easily calculated from the measurements. Anyhow, both parameters are comparable to literature data [58,60], showing stable device performance and typical charge transport processes. Furthermore, all the values are in the same order of magnitude, which is another confirmation of the method reproductivity.

Table 2
Selected parameters obtained from fitting the impedance spectra of the investigated DSSC recorded under different experimental conditions by applying the equivalent circuit presented in Fig. 7c: R_s—ohmic resistance, R_f—resistance of the TiO_2 film, R_{ce}—charge transfer resistance at the Pt/electrolyte interface, and R_{ct}—charge transfer resistance at the dye/TiO_2/electrolyte interface. Corresponding values of electron lifetime, τ_{el}, calculated from the R_{ct}-related semicircles are also included.

Voltage/V	Condition	R_s/Ω	R_f/Ω	R_{ce}/Ω	R_{ct}/Ω	τ_{el}/ms
0.7 V	dark	18.6	0.802	9.72	32.8	12.8
0.8 V	dark	18.6	1.04	6.72	14.3	7.06
0.7 V	light	18.7	1.04	7.55	17.2	8.02
0.8 V	light	18.7	1.09	5.67	9.17	5.71

4. Conclusions

Reproducible method for preparation of titania nanoparticles was proposed. The usage of chelating agent EDTA-Na_2 and the nonionic surfactant Triton X100 in the reaction mixture, during the sol-gel/hydrothermal process, has resulted in sub–25 nm particles with rice-like shape. The particles were stabilized through the formation of micelles, typical for Triton X100. Due to dense micellar packing, the micelles were broken using ultrasound and processed into monolith mesoporous thick films, more favorable from the perspective of photovoltaic application. The XRD and SAED of scratched film sample confirmed the presence of desirable anatase crystallographic phase, also confirmed by the optical band-gap calculations (3.17 eV). The N_2 adsorption/desorption measurement revealed mesoporosity with non-uniform distribution curve and 158 m^2/g specific surface area. The films exhibited crack-free structure, with superior adhesion, as a result of the optimization of paste composition, calcination profile and the impregnation using $TiCl_4$ treatment.

The films with thickness of 6 μm were used to fabricate circular 0.24 cm^2 DSSC, with a solar-to-electric power conversion efficiency up to 5.22%, under 100 mW·cm^{-2} of halogen illumination. Considering that we have used the simplest possible cell configuration (without additional functional layers that somewhat enhance efficiency, but also increase the fabrication expenses), the obtained reproductive photovoltaic parameters are excellent base for future innovations and possible commercialization. The next idea would certainly be usage of more efficient dyes, perhaps novel silyl-anchor and carboxy-anchor dyes, which exhibit much higher efficiencies in comparison to traditional Ru-dyes [3]. Another idea would be to explore the applicability of as prepared particles and films in wide range of other practical purposes, such as photocatalysis, water splitting, hydrogen production etc.

Acknowledgements

The authors acknowledge that this work was financially supported by the Serbian Ministry of Education, Science and Technological Development through the project No. III45007, and the Bilateral Project between the Republic of Serbia and Republic of

Slovenia, under No. 451-03-3095/2014-09-32. The TEM work was conducted in the infrastructure Centre for Electron Microscopy and Microanalysis (CEMM) at Jožef Stefan Institute, Ljubljana (Slovenia).

Appendix A. Supplementary data

Supplementary data associated with this article can be found, in the online version, at http://dx.doi.org/10.1016/j.electacta.2016.05.179.

References

[1] B. O'Regan, M. Gratzel, A low-cost, high-efficiency solar cell based on dye-sensitized colloidal TiO_2 films, Nature 353 (1991) 737.
[2] M. Gratzel, Recent Advances in Sensitized Mesoscopic Solar Cells, Accounts Chem. Res. 42 (2009) 1788.
[3] K. Kakiage, Y. Aoyama, T. Yano, K. Oya, J.-I. Fujisawa, M. Hanaya, Highly-efficient dye-sensitized solar cells with collaborative sensitization by silyl-anchor and carboxy-anchor dyes, Chem. Commun. (2015), doi:http://dx.doi.org/10.1039/C5CC06759F Advanced Article.
[4] M.A. Green, K. Emery, Y. Hishikawa, W. Warta, E.D. Dunlop, Solar cell efficiency tables (Version 44), Prog. Photovoltaics 22 (2014) 701.
[5] H.J. Snaith, Estimating the Maximum Attainable Efficiency in Dye-Sensitized Solar Cells, Adv. Funct. Mater. 20 (2010) 13.
[6] L. Peter, The Gratzel Cell: Where Next? J. Phys. Chem. Lett. 2 (2011) 1861.
[7] L. Wang, X. Fang, Z. Zhang, Design methods for large scale dye-sensitized solar modules and the progress of stability research, Renew. Sust. Energy Rev. 14 (2010) 3178.
[8] M. Ye, X. Wen, M. Wang, J. Iocozzia, N. Zhang, C. Lin, Z. Lin, Recent advances in dye-sensitized solar cells: from photoanodes, sensitizers and electrolytes to counter electrodes, Mater. Today 18 (2015) 155.
[9] A. Yella, H.N. Lee, C. Tsao, A.K. Yi, M.K. Chandiran, E.W.-G. Diau, -Y.-S.M. Yeh, M. Gratzel, orphyrin-Sensitized Solar Cells with Cobalt (II/III)-Based Redox Electrolyte Exceed 12 Percent Efficiency, Science 334 (2011) 629.
[10] K. Mietunnen, J. Halme, P. Lund, Metallic and plastic dye solar cells, WIREs Energy Environ. 2 (2013) 104.
[11] J. Zhi, H. Cui, A. Chen, Y. Xie, F. Huang, Efficient highly flexible dye sensitized solar cells of three dimensional graphene decorated titanium dioxide nanoparticles on plastic substrate, J. Power Sources 281 (2015) 404.
[12] Y. Liu, H. Xu, H. Wang, W. Zhao, C. Liang, M. Zhong, H. Shen, Flexible TiO_2 nanotube-based dye-sensitized solar cells using laser-drilled microhole array electrodes, Appl. Phys. A 102 (2011) 127.
[13] C.J. Wood, G.H. Summers, E.A. Gibson, Increased photocurrent in a tandem dye-sensitized solar cell by modifications in push–pull dye-design, Chem. Commun. 51 (2015) 3915.
[14] R. Tagliaferro, D. Gentilini, S. Mastroianni, A. Zampetti, A. Gagliardi, T.M. Brown, A. Reale, A. Di Carlo, Integrated tandem dye solar cells, RSC Adv. 3 (2013) 20273.
[15] M. Gratzel, Sol-Gel Processed TiO_2 Films for Photovoltaic Applications, J. Sol-Gel Sci. Technol. 22 (2001) 7.
[16] S.S. Mali, C.A. Betty, P.N. Bhosale, P.S. Shinde, M.R. Pramod, S.R. Jadkar, P.S. Patil, Efficient dye-sensitized solar cells based on hierarchical rutile TiO_2 microspheres, CrystEngComm 14 (2012) 8156.
[17] V.M. Mohan, K. Murakami, Hydrothermal Synthesis of TiO_2 Porous Hollow Nanospheres for Coating on the Photoelectrode of Dye-Sensitized Solar Cells, Jpn. J. Appl. Phys. 51 (2012) 02BP11-1-6.
[18] C.-C. Tsai, H. Teng, Structural Features of Nanotubes Synthesized from NaOH Treatment on TiO_2 with Different Post-Treatments, Chem. Mater. 18 (2006) 367.
[19] H. Chang, Y.-L. Chen, Preparation of Multilayer TiO_2 Thin Films for Dye-sensitized Solar Cells, Jpn. J. Appl. Phys. 49 (2010) 06GG04-1-6.
[20] C.J. Barbe, F. Arendse, P. Comte, M. Jirousek, F. Lenzmann, V. Shklover, M. Gratzel, Nanocrystalline Titanium Oxide Electrodes for Photovoltaic Applications, J. Am. Ceram. Soc. 80 (1997) 3157.
[21] S.D. Burnside, V. Shklover, C. Barbe, P. Comte, F. Arendse, K. Brooks, M. Gratzel, Self-Organization of TiO_2 Nanoparticles in Thin Films, Chem. Mater. 10 (1998) 2419.
[22] X. Wang, Y. Liu, X. Zhou, B. Li, H. Wang, W. Zhao, H. Huang, C. Liang, X. Yu, Z. Liu, H. Shen, Synthesis of long TiO_2 nanowire arrays with high surface areas via synergistic assembly route for highly efficient dye-sensitized solar cells, J. Mater. Chem. 22 (2012) 17531.
[23] M.M. Rashad, A.E. Shalan, Surfactant-assisted hydrothermal synthesis of titania nanoparticles for solar cell applications, J. Mater. Sci. Mater. Electron. 24 (2013) 3189.
[24] M.S. Muniz, J.J. Goes, J.A. Silva, E. Varela, R. Joanni, Synthesis and characterization of mesoporous TiO_2 nanostructured films prepared by a modified sol–gel method for application in dye solar cells, Ceram. Int. 37 (2011) 1017.
[25] H.-Y. Koo, Y.J. Kim, Y.H. Lee, W.I. Lee, K. Kim, N.-G. Park, Nano-embossed Hollow Spherical TiO_2 as Bifunctional Material for High-Efficiency Dye-Sensitized Solar Cells, Adv. Mater. 20 (2008) 195.
[26] D. Chen, F. Huang, Y.-B. Cheng, R.A. Caruso, Mesoporous Anatase TiO_2 Beads with High Surface Areas and Controllable Pore Sizes: A Superior Candidate for High-Performance Dye-Sensitized Solar Cells, Adv. Mater. 21 (2009) 2206.
[27] A.U. Ubale, Y.S. Sakhare, S.M. Bombatkar, Influence of the complexing agent (Na_2-EDTA) on the structural, morphological, electrical and optical properties of chemically deposited FeSe thin films, Mater. Res. Bull. 48 (2013) 3564.
[28] J.-H. Ha, P. Muralidharan, D.K. Kim, Hydrothermal synthesis and characterization of self-assembled h-WO_3 nanowires/nanorods using EDTA salts, J. Alloy. Compd. 475 (2009) 446.
[29] F. Luo, C.-J. Jia, W. Song, L. -P- You, C. -H- Yan, Chelating Ligand-Mediated Crystal Growth of Cerium Orthovanadate, Cryst. Growth Des. 5 (2005) 137.
[30] J. Ma, Q. Wu, Y. Ding, Mild hydrothermal solid-phase synthesis of YVO_4 nanocrystals, Mater. Lett. 61 (2007) 3616.
[31] W. N. Wang, Q. Chen, Y. Dai Zhang, Synthesis, luminescent, and magnetic properties of $LaVO_4$:Eu nanorods, Mater. Lett. 62 (2008) 109.
[32] Y. Xiong, M. Wu, J. Ye, Q. Chen, Synthesis and luminescence properties of hand-like α-Bi_2O_3 microcrystals, Mater. Lett. 62 (2008) 1165.
[33] Z. Zhang, Y. Fu, C. Zhou, J. Li, Y. Lai, EDTA-Na_2-assisted hydrothermal synthesis of Cu_2SnS_3 hollow microspheres and their lithium ion storage performances, Solid State Ionics 269 (2015) 62.
[34] L. Qi, J.D. Sorge, D.P. Birnie III, Dye-Sensitized Solar Cells Based on TiO_2 Coatings with Dual Size-Scale Porosity, J. Am. Ceram. Soc. 92 (2009) 1921.
[35] J.-G. Nam, E.-S. Lee, W.-C. Jung, Y.-J. Park, B.-H. Sohn, S.-C. Park, J.S. Kim, J.-Y. Bae, Photovoltaic enhancement of dye-sensitized solar cell prepared from [TiO_2/ethyl cellulose/terpineol] paste employing TRITON^{TM} X-based surfactant with carboxylic acid group in the oxyethylene chain end, Mater. Chem. Phys. 116 (2009) 46.
[36] S.N. Karthick, K.V. Hemalatha, C.J. Raj, A. Subramania, H.-J. Kim, Preparation of TiO_2 paste using poly(vinylpyrrolidone) for dye sensitized solar cells, Thin Solid Films 520 (2012) 7018.
[37] N. Tasić, Z. Branković, Z. Marinković Stanojević, G. Branković, Effect of Binder Molecular Weight on Morphology of TiO_2 Films Prepared by Tape Casting and Their Photovoltaic Performance, Sci. Sinter. 44 (2012) 365.
[38] S. Ito, P. Chen, P. Comte, M.K. Nazeeruddin, P. Liska, P. Pechy, M. Gratzel, Fabrication of Screen-Printing Pastes From TiO_2 Powders for Dye-Sensitised Solar Cells, Prog. Photovoltaics 15 (2007) 603.
[39] P.M. Sommerling, B.C. O'Regan, R.R. Haswell, H.J.P. Smit, N.J. Bakker, J.J.T. Smits, J.M. Kroon, J.A.M. van Roosmalen, Influence of a TiCl4 Post-Treatment on Nanocrystalline TiO_2 Films in Dye-Sensitized Solar Cells, J. Phys. Chem. B 110 (2006) 19191.
[40] B.C. O'Regan, J.R. Durrant, P.M. Sommerling, N.J. Bakker, Influence of the $TiCl_4$ Treatment on Nanocrystalline TiO_2 Films in Dye-Sensitized Solar Cells. 2. Charge Density, Band Edge Shifts, and Quantification of Recombination Losses at Short Circuit, J. Phys. Chem. C 111 (2007) 14001.
[41] F. Rouquerol, J. Rouquerol, K.S.W. Sing, P. Llewellyn, G. Maurin, Adsorption by Powders and Porous Solids, Principles, Methodology and Applications, Academic Press, New York, 2012.
[42] B.C. Lippens, B.G. Linsen, J.H. de Boer, Studies on pore systems in catalysts I. The adsorption of nitrogen; apparatus and calculation, J. Catal. 3 (1964) 32.
[43] K. Sing, D. Everet, R. Haul, L. Moscou, R. Pierotti, J. Rouquerol, T. Siemieniewska, Reporting physisorption data for gas/solid systems with special reference to the determination of surface area and porosity (Recommendations 1984), Pure Appl. Chem. 57 (1985) 603.
[44] C.F. Brinker, G.W. Scherer, Sol-gel science, The Physics and Chemistry of Sol-Gel Processing, Academic Press, New York, 1990.
[45] A.P. Mishra, R. Khan, R.R. Pandey, Kinetic studies on effects of EDTA and surfactants on reduction of vanadium(V) to vanadium(IV) in suphuric acid medium, Indian J. Chem. A 48 (2009) 1228.
[46] N.-G. Park, J. van de Lagemaat, A.J. Frank, Comparison of Dye-Sensitized Rutile- and Anatase-Based TiO_2 Solar Cells, J. Phys. Chem. B 104 (2010) 8989.
[47] P. Kubelka, F. Munk, An Article on Optics of Paint Layers, Z. Tech. Phys. 12 (1931) 593.
[48] J. Tauc, R. Grigorovici, A. Vancu, Optical Properties and Electronic Structure of Amorphous Germanium, Phys. Status Solidi 15 (2006) 627.
[49] R. Kawakami, Y. Sato, Y. Mori, S. Yoshikado, Composite thin films prepared by electrophoresis using two types of TiO_2 nanoparticles, J. Ceram. Soc. Jpn. 122 (2014) 436.
[50] Q. Wang, J.-E. Moser, M. Gratzel, Electrochemical Impedance Spectroscopic Analysis of Dye-Sensitized Solar Cells, J. Phys. Chem. B 109 (2005) 14945.
[51] F. Fabregat-Santiago, J. Bisquert, E. Palomares, L. Otero, D. Kuang, S.M. Zakeeruddin, M. Gratzel, Correlation between photovoltaic performance and impedance spectroscopy of dye-sensitized solar cells based on ionic liquids, J. Phys. Chem. C 111 (2007) 6550.
[52] H. Xu, X. Tao, D.-T. Wang, Y.-Z. Zheng, J.-F. Chen, Enhanced efficiency in dye-sensitized solar cells based on TiO_2 nanocrystal/nanotube double-layered films, Electrochim.Acta 55 (2010) 2280.
[53] Y.P. Lin, S.Y. Lin, Y.C. Lee, Y.W. Chen-Yang, High surface area electrospun prickle-like hierarchical anatase TiO_2 nanofibers for dye-sensitized solar cell photoanodes, J. Mater. Chem. A 1 (2013) 9875.
[54] H. Yu, S. Zhang, H. Zhao, G. Will, P. Liu, An efficient and low-cost TiO_2 compact layer for performance improvement of dye-sensitized solar cells, Electrochim. Acta 54 (2009) 1319.

[55] Z.-H. Liu, X.-J. Su, G.-L. Hou, S. Bi, Z. Xiao, H.-P. Jia, Enhanced performance for dye-sensitized solar cells based on spherical TiO_2 nanorod-aggregate light-scattering layer, J. Power Sources 218 (2012) 280.
[56] A. Zaban, M. Greenshtein, J. Bisquert, Determination of Electron Lifetime in Nanocrystalline Dye Solar Cells by Open-Circuit Voltage Decay Measurements, Chemphyschem 4 (2003) 859.
[57] J. Bisquert, A. Zaban, M. Greenshtein, I. Mora-Sero, Determination of Rate Constants for Charge Transfer and the Distribution of Semiconductor and Electrolyte Electronic Energy Levels in Dye-Sensitized Solar Cells by Open-Circuit Photovoltage Decay Method, J. Am. Chem. Soc. 126 (2004) 13550.
[58] G.K. Mor, K., Shankar, M., Paulose, O.K., Varghese, C.A. Grimes, Use of Highly-Ordered TiO_2 Nanotube Arrays in Dye-Sensitized 6 (2005) 215.
[59] D. Zhao, T. Peng, L. Lu, P. Cai, P. Jiang, Z. Bian, Effect of Annealing Temperature on the Photoelectrochemical Properties of Dye-Sensitized Solar Cells Made With Mesoporous TiO_2 Nanoparticles, J. Phys. Chem. C 112 (2008) 8486.
[60] M. Sajedi Alvar, M. Javadi, Y. Abdi, E. Arzi, Enhancing the electron lifetime and diffusion coefficient in dye-sensitized solar cells by patterning the layer of TiO_2 nanoparticles, J. Appl. Phys. 119 (2016) 114302.
[61] A.B.F. Martinson, M.S. Goes, F. Fabregat-Santiago, J. Bisquert, M.J. Pellin, J.T. Hupp, Electron Transport in Dye-Sensitized Solar Cells Based on ZnO Nanotubes: Evidence for Highly Efficient Charge Collection and Exceptionally Rapid Dynamics, J. Phys. Chem. A 113 (2009) 4015.